

# Multi-Scale Coarse-to-Fine Segmentation for Screening Pancreatic Ductal Adenocarcinoma

Zhuotun Zhu<sup>\*,1</sup>, Yingda Xia<sup>\*,1</sup>,  
Lingxi Xie<sup>1</sup>, Elliot K. Fishman<sup>2</sup>, Alan L. Yuille<sup>1</sup>

<sup>1</sup>The Johns Hopkins University, Baltimore, MD 21218, USA

<sup>2</sup>The Johns Hopkins University School of Medicine, Baltimore, MD 21287, USA  
zhuotun@gmail.com philyingdaxia@gmail.com 198808xc@gmail.com  
efishman@jhmi.edu alan.l.yuille@gmail.com

**Abstract.** This paper proposes an intuitive approach to finding pancreatic ductal adenocarcinoma (PDAC), the most common type of pancreatic cancer, by checking abdominal CT scans. Our idea is named *segmentation-for-classification* (S4C), which classifies a volume by checking if at least a sufficient number of voxels is segmented as the tumor. In order to deal with tumors with different scales, we train volumetric segmentation networks with **multi-scale** inputs, and test them in a **coarse-to-fine** flowchart. A post-processing module is used to filter out outliers and reduce false alarms. We perform a case study on our dataset containing 439 CT scans, in which 136 cases were diagnosed with PDAC and 303 cases are normal. Our approach reports a sensitivity of 94.1% at a specificity of 98.5%, with an average tumor segmentation accuracy of 56.46% over all PDAC cases.

## 1 Introduction

Pancreatic cancer is one of the most dangerous killers to human lives, causing more than 330,000 deaths globally in 2014 [11]. Pancreatic ductal adenocarcinoma (PDAC) is the most common type of pancreatic cancer, accounting for about 85% of cancer cases. In early stages, this disease often has few symptoms and is very difficult to discover. By the time of diagnosis, the cancer has often spread to other parts of the body, leading to a very poor prognosis (*e.g.*, a five-year survival rate of 5% [11]). But, for cases diagnosed early, the survival rate rises to about 20% [7]. Hence, it is very important to study the possibility of detecting PDAC in common examinations, *e.g.*, the abdominal CT scan.

The early diagnosis of pancreatic cancer requires much expertise in reading the scanned images and making decisions, but the increasing number of cases makes it impossible for a limited number of experienced radiologists to check all CT scans manually. Therefore, an artificial intelligence system for this purpose is in need. In particular, the radiologists in our team are interested in a system

---

\* The first two authors equally contributed to the work.

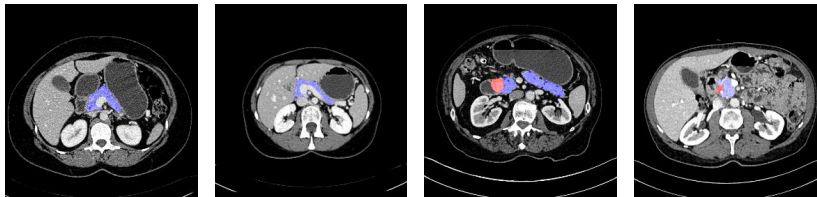


**Fig. 1.** Examples of normal and abnormal (PDAC) pancreases (best viewed in color). Blue and red region mark the pancreas and tumor, respectively. The tumor sizes vary a lot in the PDAC cases (we show a medium-sized one and a small-sized one).

working on abdominal CT scans, which filters out a large fraction of normal cases, but preserves almost all abnormal cases for further investigation. To the best of our knowledge, there is no existing work on this task.

This problem falls into the area of computer-assisted diagnosis (CAD). With the development of deep learning, in particular the state-of-the-art convolutional neural networks for image recognition [5][3], it is possible to construct a system which learns from professional knowledge in data annotation, and apply it to helping doctors in various clinical purposes. The pancreas is one of the most challenging organs in CT segmentation [9]. The difficulty mainly lies in its irregular shape and low contrast around the boundary. Powered by the recent progress in deep learning for 2D [1][8] and 3D [6][12][18] image segmentation, researchers designed various approaches [10][16] towards accurate pancreas segmentation. In the pathological cases, the morphology of the pancreas can be largely impacted by the difference in the pancreatic cancer stage [14], making it more difficult to segment the pancreas and lesion areas accurately [15].

This paper is aimed at detecting PDAC from a mixed set of normal and abnormal CT scans. This is a classification task [2][4], but we suggest an alternative solution named *segmentation-for-classification* (S4C), which trains segmentation models and uses their outputs for classification. To deal with tumors of various sizes (see Figure 1), we design deep segmentation network with multiple input scales, *i.e.*,  $64^3$ ,  $32^3$  and  $16^3$  volumes. But, voting that small input regions lead to a high false alarm rate, we adopt a **coarse-to-fine** testing strategy, which uses the  $64^3$  network for a coarse scan, and then uses the  $32^3$  and  $16^3$  networks inside the bounding box to find small tumors that are possibly ignored in the coarse segmentation. A non-parameterized post-processing algorithm is designed to filter out outliers. A testing volume is classified as PDAC (abnormal) if at least 50 voxels are segmented as tumor.

We perform experiments on our own dataset with a mixture of normal and abnormal CT scans. In tumor segmentation, our multi-scale approach achieves an average DSC of 56.46% over 136 cases. In classification, we miss 8 out of 136 abnormal cases (sensitivity is 94.1%), and false-alarm 3 of 200 normal cases (specificity is 98.5%). Both the classification and segmentation results can assist the radiologists in further investigation, and largely reduce their workload.

## 2 The Segmentation-for-Classification Approach

### 2.1 The Overall Framework

Let a dataset be  $\mathbf{S} = \{(\mathbf{X}_1, y_1^*), \dots, (\mathbf{X}_N, y_N^*)\}$ , where  $N$  is the number of CT scans,  $\mathbf{X}_n \in \mathbb{R}^{W_n \times H_n \times L_n}$  is the 3D volume with each element indicating the Hounsfield unit (HU) of a voxel, and  $y_n \in \{0, 1\}$  is the label (0 for a normal case, 1 for an abnormal case). Throughout this paper, by *abnormal* we refer to the cases diagnosed as PDAC. The goal is to design a model  $\mathbb{M} : y = f(\mathbf{X})$  to predict the label for each testing volume. We evaluate our approach by ranking all volumes by the probability of being a PDAC, computing the sensitivity and specificity at a given threshold, and plotting the ROC curve indicating the relationship between the sensitivity and specificity at different thresholds. For clinical purposes, we shall guarantee a high sensitivity (few PDAC cases are missed) with a reasonable specificity (there are not too many false alarms).

Although some previous work suggested to classify CT or MRI volumes directly using 3D networks [2][4], we argue that a better solution is to perform tumor segmentation at the same time of classification. This makes the classification results **interpretable** by segmentation cues, by which radiologists can take a further investigation of the suspicious abnormal regions. In addition, this integrates voxel-wise annotations into the classification model as deep supervision, so that the entire network is better trained [15]. Therefore, we propose a two-stage framework named *segmentation-for-classification*, in which a segmentation stage first extracts voxel-wise cues from the input CT scan, and a classification stage follows to summarize these information into the final prediction. Our multi-scale segmentation strategy is different from [17], which applied another network of the same scale in the fine stage. **Tumor detection requires multiple scales.**

Mathematically, let each training data be augmented by a segmentation mask  $\mathbf{M}_n^*$  of the same dimensionality as  $\mathbf{X}$ , so that  $m_{n,i}^* \in \{0, 1, 2\}$  indicates the category of the  $i$ -th voxel, *i.e.*, in the tumor ( $m_{n,i} = 2$ ), outside the tumor but inside the pancreas ( $m_{n,i} = 1$ ), or outside the pancreas ( $m_{n,i} = 0$ ). Note that the tumor voxel set is a subset of the pancreas voxel set. The segmentation module is a high-dimensional function  $\mathbf{M} = \mathbf{s}(\mathbf{X})$ , which is implemented by a deep encoder-decoder network. The classification module is a binary function  $y = c(\mathbf{M})$ . The overall framework is thus written as:

$$y = f(\mathbf{X}) = c \circ \mathbf{s}(\mathbf{X}). \quad (1)$$

### 2.2 Training: Multi-Scale Deeply-Supervised Segmentation

We start with describing the segmentation stage. The tumor region in a pancreas, as shown in Figure 1, can vary in scale, appearance and geometric properties. In particular, the largest tumor in our dataset occupies over one million voxels, but the smallest one has only thousands. This motivates us to train multi-scale networks to deal with such a large variation in scale.

In practice, we train three networks, taking input volumes of  $64^3$ ,  $32^3$  and  $16^3$  voxels, respectively. Each segmentation network follows an encoder-decoder

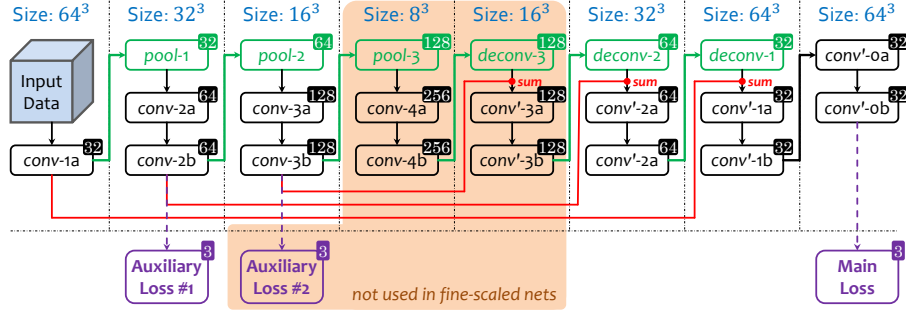


**Fig. 2.** The architecture of a 3D deeply-supervised segmentation network (best viewed in color). Each rectangle is a layer, green arrows indicate operations changing spatial resolution, and red arrows mean residual connections. We display the situation when the input volume size is  $64^3$ . If it is changed to  $32^3$  or  $16^3$ , all volumes are shrunk accordingly (to  $1/2^3$  or  $1/4^3$  of the displayed size). The number at the upper-right corner of each cube is the number of channels. Each convolution uses  $3 \times 3 \times 3$  kernels with a stride of 1, each pooling  $2 \times 2 \times 2$  with a stride of 2 (down-sampling by 2), and each deconvolution  $4 \times 4 \times 4$  with a stride of 2 (up-sampling by 2). Batch-normalization and ReLU activation are used after each convolution and deconvolution. The loss function works by first up-sampling the cube to the output size via deconvolution, followed by a  $1 \times 1 \times 1$  convolution, and then computing the voxel-wise cross-entropy loss. The weight ratio for auxiliary losses #1, #2 and the main loss is  $1 : 2 : 5$  for the  $64^3$  network, and  $1 : 3$  for the auxiliary loss #1 and the main loss for the  $32^3$  and  $16^3$  networks.

flowchart shown in Figure 2. It has a series of convolutional layers to learn 3D patterns from training data. Down-sampling and up-sampling are implemented by max pooling and deconvolutional layers, respectively. Following [17], we introduce deep supervision in the training process, which is implemented by adding several auxiliary losses to intermediate layers. Deep supervision is considered as a way of incorporating multi-stage visual cues [13], which constrains intermediate layers and improves the stability of training deep networks. Multi-scale segmentation is complementary to deep supervision, which aims at capturing visual patterns of various scales. As can be seen in experiments, multi-scale segmentation can take advantage of different scales, *i.e.*, a large network produces a higher specificity, and a small network enjoys a higher sensitivity.

The training process starts with sampling patches of a specified size. Since the pancreas and the tumor only occupy a small fraction of the entire volume, a random sampling strategy may lead to that only few patches contain pancreas or tumor voxels, and thus the segmentation models are biased towards the background class. To deal with the issue, we sample lots of foreground patches for training the  $32^3$  and  $16^3$  networks. We first compute the region-of-interest (ROI) by padding a 32-voxel margin around the minimal 3D bounding box covering the entire pancreas. Within it, we categorize the randomly sampled patches into three types (*i.e.*, *background*, *tumor* and *pancreas*) according to the fraction of pancreas and tumor voxels, and make the numbers of training patches

of these types to be approximately the same. Data augmentation is performed by randomly flipping patches and rotating by  $90^\circ$ ,  $180^\circ$  and  $270^\circ$  over three axes.

We use the same configuration for training these networks. The base learning rate is 0.01 and decayed polynomially (the power is 0.9) in a total of 80,000 iterations (the mini-batch size is 16, 32 and 128 for  $64^3$ ,  $32^3$  and  $16^3$ , respectively). The weight decay and momentum are set to be 0.0005 and 0.9, respectively.

### 2.3 Testing: Coarse-to-Fine Segmentation with Post-Processing

The first goal in the testing stage is to perform the pancreas and tumor segmentation. We first slide a  $64^3$  window in the entire CT volume. The spatial stride is 20 along three axes, which is chosen to limit the average testing time for each case within 11 minutes. Based on the *coarse* segmentation, we compute the ROI, *i.e.*, the smallest box covering all pancreas and tumor voxels padded by 32, and crop the CT image accordingly. Then, we scan the ROI with sliding windows of  $32^3$  and  $16^3$  voxels, and the strides are set to be 10 and 5, respectively. We do not run the two small networks on the entire volume because it can easily hallucinate tumors in the background regions. In addition, shrinking the scanning region for the  $32^3$  and  $16^3$  networks leads to a significant speedup in the testing process. The predictions of three networks are averaged into final segmentation.

Then, based on the segmentation mask, we classify each volume as normal or abnormal. Advised by the radiologists who desire the classification result to be explainable, we do not formulate the classifier  $c(\cdot)$  as another deep network, but use a simple, non-parametrized approach to filter out the outliers. We construct a graph on all voxels predicted as *normal pancreas* or *tumor*. Each voxel is a node, and there exists an edge between the adjacent voxels (each voxel is adjacent to 6 neighbors). We compute all connected component in the graph. A component is preserved if it is larger than 20% of the maximal connected component, otherwise it is removed, *i.e.*, all voxels within this component are predicted as *background*.

Finally, a volume is predicted as PDAC if at least  $K$  voxels are predicted as tumor. In practice, we set  $K = 50$ . It is worth noting that our method is not sensitive to  $K$ . Even setting  $K = 1500$  does not change our results and observations too much.

## 3 Experiments

### 3.1 Dataset and Settings

We collected a dataset with 303 normal cases from potential renal donors, as well as 136 biopsy-proven PDAC cases. Four experts in abdominal anatomy annotated the pancreas and tumor voxels on these data using the Varian Velocity software, and each case was checked by a experienced board certified Abdominal Radiologist. For a radiologist, an average normal case took 20 minutes, and an average abnormal case 40 minutes to segment. Since the abnormal cases are much harder to obtain and annotate than the normal cases, we adopt a

Scale	N. Pancreas	A. Pancreas	Tumor	Misses	Sens.	Spec.
$64^3$	<b>86.90</b> $\pm$ 8.57%	<b>80.98</b> $\pm$ 10.75%	<b>57.25</b> $\pm$ 28.05%	10/136	92.7%	<b>99.0%</b>
$32^3$	82.01 $\pm$ 12.21%	75.66 $\pm$ 19.92%	53.84 $\pm$ 26.08%	7/136	94.9%	96.0%
$16^3$	61.53 $\pm$ 20.64%	64.14 $\pm$ 20.16%	42.53 $\pm$ 26.63%	4/136	<b>97.1%</b>	86.5%
Multi	84.52 $\pm$ 11.11%	78.60 $\pm$ 18.34%	56.46 $\pm$ 26.23%	8/136	94.1%	98.5%

**Table 1.** Comparison of segmentation and classification results by networks of different scales and their combination. From left to right: normal/abnormal pancreas and tumor segmentation accuracy (DSC, %), the number of missing tumors (*i.e.*, DSC is 0%), and the sensitivity ( $= 1 - \text{miss rate}$ ) and specificity. Results of the  $32^3$  and  $16^3$  networks are based on the predicted bounding box provided by the  $64^3$  network, otherwise the segmentation accuracy is much lower due to a large number of false positives.

4-fold cross-validation on our 136 PDAC scans to have testing results on every abnormal case while we use a hard split of training and testing on our 303 normal cases. All in all, each training set contains 103 normal and 102 abnormal cases where the normal-to-abnormal ratio is fairly close to 1, and each testing set contains 34 abnormal and 200 normal cases. The average size over all CT scans is  $512 \times 512 \times 667$ .

One of our goals is to measure the segmentation accuracy by the Dice-Sørensen Coefficient (DSC) between the predicted and the ground-truth tumor sets  $\mathcal{Y}$  and  $\mathcal{Y}^*$ , *i.e.*,  $\text{DSC}(\mathcal{Y}, \mathcal{Y}^*) = \frac{2 \times |\mathcal{Y} \cap \mathcal{Y}^*|}{|\mathcal{Y}| + |\mathcal{Y}^*|}$ . Our main goal is the abnormality classification, which involves a tradeoff between sensitivity (the fraction of correctly classified abnormal cases) and specificity (the fraction of correctly classified normal cases).

### 3.2 Segmentation Results

We first summarize the segmentation results in Table 1. The  $64^3$  network achieves reasonable pancreas and tumor segmentation accuracies. The segmentation result of normal pancreas is as high as 86.90%, which means that the normal pancreases are easier to segment, as there are often unpredicted changes in shape and geometry in the abnormal cases. As a side comment, the lowest DSC of an abnormal pancreas is 38.40%, lower than the number (44.03%) of a normal pancreas. In tumor segmentation, we observe a lower accuracy and a higher standard deviation ( $57.25 \pm 28.05\%$ ). Except for the 10 missing cases, we find 20 more cases with a tumor DSC lower than 30%. All these evidences imply the challenging of finding tumors especially when they are small.

Going to smaller scales, fewer tumors are missed, but segmentation accuracies for both pancreas and tumor become lower. This raises the tradeoff between sensitivity and specificity – a network with a smaller input region has the ability of detecting tiny regions, but without seeing contexts, it can be easily confused by the false positives. Therefore, combining multi-scale predictions achieves a balance between sensitivity and specificity. Figure 3 shows two typical examples that benefit from multi-scale segmentation.

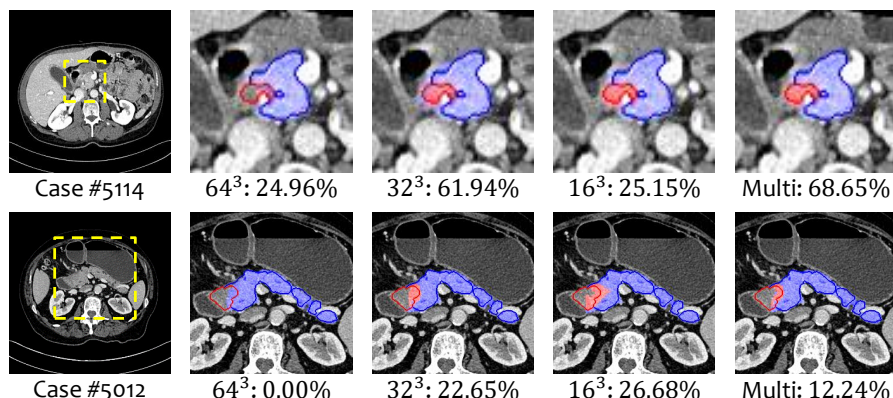


**Fig. 3.** Multi-scale segmentation examples (best viewed in color). Top: a case that all three scales work well, and multi-scale combines them to achieve a higher DSC. Bottom: a failure case in the  $64^3$  network, but found by the  $32^3$  and  $16^3$  networks. The yellow frames indicate the zoomed-in regions, the blue and red contours mark the annotated pancreas and tumor respectively, and the masked regions mark segmentation results.

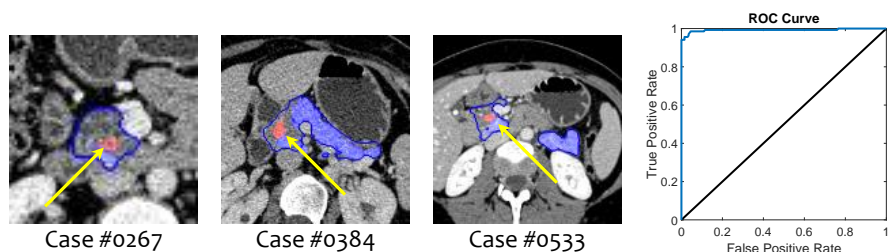


**Fig. 4.** Left: three false alarm examples, in which the blue contour marks the annotated pancreas, and the blue and red regions mark the predicted pancreas and tumor, respectively. We use yellow arrows to indicate the detected tiny “tumors”. Right: the ROC curve of multi-scale classification. This figure is best viewed in color.

### 3.3 Classification Results

Finally, we summarize classification results in Table 1. Radiologists care more about a high sensitivity since they don’t want to miss a patient who has an abnormal pancreas, which inspires us to adopt a multi-scale strategy to improve the sensitivity while keeping a reasonable specificity. The model with multi-scale information achieves the best overall performance, *i.e.*, a sensitivity of 94.1% (128/136) at a specificity of 98.5% (197/200). These high scores imply that tumor segmentation provide strong cues for PDAC screening. We show all three false alarms in Figure 4. The radiologists of our team confirmed that 2 out of these 3 false positives have focal fatty infiltration in the pancreas corresponding to the detected “tumors”. Focal fatty infiltration can be difficult for the radiologist to

distinguish from tumor in current clinical practice. In this case, the predicted “false alarm” was indeed not normal in view of our radiologists on the CT scan.

Our approach can output a confident score in  $[0, 1]$  for each case, indicating the probability that this case suffers PDAC. This score is computed by a weighted sum of the number of tumor voxels and the average segmentation probability of all tumor voxels. Sorting all cases according to their confident scores obtains a ROC curve of sensitivity and specificity. We can also tune the classification threshold to change the tradeoff between sensitivity and specificity, *e.g.*, we can achieve a sensitivity of 98.5% at a specificity of 95.6%, or a specificity of 99.5% at a sensitivity of 94.1%.

## 4 Conclusions

In this paper, we study an important and challenging task, *i.e.*, detecting pancreases suffering from PDAC in abdominal CT scans. This topic is crucial in saving lives from pancreatic cancer yet few studied before, possibly due to the lack of data. We propose a *segmentation-for-classification* (S4C) framework which trains a segmentation network and performs abnormality classification by simply checking the existence of tumor voxels in each testing volume. There are two key points to improve classification accuracy, known as **multi-scale** network training and **coarse-to-fine** testing. In a dataset containing 303 normal and 136 PDAC cases, we achieve an average tumor segmentation accuracy of over 56%, and a sensitivity of 94.1% at a specificity of 98.5%. These strong numbers show promise in clinics.

Our approach enjoys another benefit that producing interpretable predictions, which reduces the workload of human doctors. In the future, we will combine other cues (*e.g.*, the shape of the pancreas) into our framework, and explore a joint way of optimizing segmentation and classification.

## References

1. Chen, L.C., Papandreou, G., Kokkinos, I., Murphy, K., Yuille, A.L.: Deeplab: Semantic image segmentation with deep convolutional nets, atrous convolution, and fully connected crfs. In: ICLR (2016)
2. Dou, Q., Chen, H., Yu, L., Qin, J., Heng, P.A.: Multilevel contextual 3-d cnns for false positive reduction in pulmonary nodule detection. IEEE TBE 64(7), 1558–1567 (2017)
3. He, K., Zhang, X., Ren, S., Sun, J.: Deep residual learning for image recognition. In: CVPR (2016)
4. Hussein, S., Chuquicusma, M.M., Kandel, P., Bolan, C.W., Wallace, M.B., Bagci, U.: Supervised and unsupervised tumor characterization in the deep learning era. arXiv:1801.03230 (2018)
5. Krizhevsky, A., Sutskever, I., Hinton, G.E.: Imagenet classification with deep convolutional neural networks. In: NIPS (2012)
6. Milletari, F., Navab, N., Ahmadi, S.A.: V-net: Fully convolutional neural networks for volumetric medical image segmentation. In: 3DV (2016)

7. PDQ Adult Treatment Editorial Board: Pancreatic cancer treatment (PDQ®) (2017)
8. Ronneberger, O., Fischer, P., Brox, T.: U-net: Convolutional networks for biomedical image segmentation. In: MICCAI (2015)
9. Roth, H.R., Lu, L., Farag, A., Shin, H.C., Liu, J., Turkbey, E.B., Summers, R.M.: Deeporgan: Multi-level deep convolutional networks for automated pancreas segmentation. In: MICCAI (2015)
10. Roth, H.R., Lu, L., Farag, A., Sohn, A., Summers, R.M.: Spatial aggregation of holistically-nested networks for automated pancreas segmentation. In: MICCAI (2016)
11. Stewart, B.W.K.P., Wild, C.P., et al.: World cancer report 2014. Health (2017)
12. Xia, Y., Xie, L., Liu, F., Zhu, Z., Fishman, E.K., Yuille, A.L.: Bridging the gap between 2d and 3d organ segmentation. MICCAI (2018)
13. Xie, S., Tu, Z.: Holistically-nested edge detection. In: ICCV (2015)
14. Zhang, L., Lu, L., Summers, R.M., Kebebew, E., Yao, J.: Personalized pancreatic tumor growth prediction via group learning. In: MICCAI (2017)
15. Zhou, Y., Xie, L., Fishman, E.K., Yuille, A.L.: Deep supervision for pancreatic cyst segmentation in abdominal ct scans. In: MICCAI (2017)
16. Zhou, Y., Xie, L., Shen, W., Wang, Y., Fishman, E.K., Yuille, A.L.: A fixed-point model for pancreas segmentation in abdominal ct scans. In: MICCAI (2017)
17. Zhu, Z., Xia, Y., Shen, W., Fishman, E.K., Yuille, A.L.: A 3d coarse-to-fine framework for automatic pancreas segmentation. arXiv:1712.00201 (2017)
18. Zhu, Z., Wang, X., Bai, S., Yao, C., Bai, X.: Deep learning representation using autoencoder for 3d shape retrieval. Neurocomputing 204, 41–50 (2016)